Clinical Science (2020) **134** 1821–1839
https://doi.org/10.1042/CS20191043

PORTLAND PRESS

Research Article

Circular RNA circFGD4 suppresses gastric cancer progression via modulating miR-532-3p/APC/β-catenin signalling pathway

Xinglong Dai, Jianjun Liu, Xiong Guo, Anqi Cheng, Xiaoya Deng, Liqun Guo and Ziwei Wang

Department of Gastrointestinal Surgery, Laboratory Research Center, The First Affiliated Hospital of Chongqing Medical University, Chongqing, 400010, PR China

Correspondence: Ziwei Wang (dxl_123abc@163.com)

Background: Mounting evidence has displayed critical roles of circular RNAs (circRNAs) in multiple cancers. The underlying mechanisms by which circFGD4 contributed to gastric cancer (GC) are still unclear.
Methods: The levels and clinical values of circFGD4 in GC patients were detected and analysed by quantitative real-time PCR. The biological roles of circFGD4 in GC were assessed *in vitro* and *in vivo* experiments. Dual-luciferase reporter, fluorescence *in situ* hybridization, RNA immunoprecipitation, biotin-coupled RNA pull-down, and TOP/Flash and FOP/Flash reporter gene assays were employed to evaluate the effects of circFGD4 on miR-532-3p-mediated adenomatous polyposis coli (APC)/β-catenin signalling in GC cells.
Results: circFGD4 expression was down-regulated the most in human GC tissues and cell lines. Low expression of circFGD4 was correlated with poor tumour differentiation, lymphatic metastasis, and poor prognosis of GC patients. circFGD4 suppressed GC cell viability, colony formation, migration, induced epithelial–mesenchymal transition (EMT), and tumorigenesis and metastasis *in vivo*. Next, we validated that circFGD4 acted as a sponge of miR-532-3p to relieve the tumour-promoting effects of miR-532-3p on its target APC. The mechanistic analysis demonstrated that the circFGD4 suppressed GC cell viability, migration, and EMT by modulating the miR-532-3p/APC axis to inactivate the β-catenin signalling.
Conclusion: circFGD4 suppressed GC progression through sponging miR-532-3p and enhancing APC expression to inactivate the β-catenin signalling. Thus circFGD4 provides a novel potential biomarker and valuable therapeutic strategy for GC.

Introduction

Gastric cancer (GC) ranks as the fifth most common malignant gastrointestinal tumours, and it is the major cause of cancer mortality not only in China but also in the world [1,2]. At present, most patients with GC are still diagnosed at an advanced stage, and the 5-year overall survival rate of GC patients remains lower than 30% [3,4]. Despite the diagnosis and therapeutic strategies continue to be enhanced, rapid proliferative capacity, lymphatic/hematogenous metastasis, and direct invasive behaviour are key factors leading to poor prognosis in GC patients. Since the occurrence and development of GC is a complex biological process, and thus far, the current molecular mechanism of GC progression has not been clearly understood [5]. The critical situation of GC diagnosis and therapy has prompted us to develop effective therapeutic strategies for anti-GC therapy and to search for valuable biomarkers to monitor GC progression.

Received: 10 October 2019
Revised: 15 June 2020
Accepted: 07 July 2020

Accepted Manuscript online: 07 July 2020
Version of Record published: 17 July 2020

Clinical Science (2020) **134** 1821–1839
https://doi.org/10.1042/CS20191043

Circular RNAs (circRNAs) are a category of non-coding RNAs (ncRNAs) formed by a closed continuous loop structure [6,7]. circRNAs are highly stable and are cell type- and tissue stage-specific, indicating that most of the circRNAs are independent of the host gene. Most recent studies have confirmed that circRNAs have multiple molecular functions, such as miRNA sponges, protein translation, and circRNA–protein interaction [8,9]. Moreover, circRNAs also play critical roles in several physiological and pathological processes, including cell cycle progression, autophagy, proliferation, invasion, metastasis, and carcinogenesis [10,11]. Nevertheless, the molecular characterizations and mechanisms of most circRNAs in human GC have not been elucidated and need further investigation. Here, circRNA microarray analysis was performed in five pairs of GC tissues to evaluate the expression of circRNAs in GC tissues and matched normal samples. Then, we screened and identified the expression and function of hsa_circ_0000390 derived from FYVE, RhoGEF and PH domain-containing 4 (FGD4) in GC and examined the underlying mechanism of hsa_circ_0000390 in GC carcinogenesis and development.

In our present study, we designed the functional and molecular experiments to examine the functional role of circFGD4 in GC. circFGD4 was markedly down-regulated in human GC tissues and cell lines and suppressed the progression and metastasis of GC cells through sponging miR-532-3p and inactivating the APC–β-catenin signalling. Importantly, low expression levels of circFGD4 were associated with poor tumour differentiation, lymph node metastasis, and poor prognosis of GC patients. The data suggest that circFGD4 serves as a tumour suppressor molecule involved in GC progression and provides an independent prognostic biomarker and target for the management of GC.

Methods

Patients data and clinical samples

All human GC tissues and noncancerous tissues from January 2013 and August 2014 were collected from the First Affiliated Hospital of Chongqing Medical University and stored in liquid nitrogen. The final diagnosis was histopathologically confirmed by two pathologists. The clinical–pathological features of all patients were recorded and are summarized in Table 1. The present study was approved by the Ethics Committee of the First Affiliated Hospital of Chongqing Medical University (Chongqing, China). Written informed consent was provided by all the participants, which agreed to participate in the present study.

CircRNA microarray analysis

Total RNAs isolated and extracted from the five human GC tissues and paired non-cancerous tissues were used for microarray analysis. RNA amplification, labelling, and hybridization with microarrays were the same as previous studies [12]. Briefly, CapitalBio circRNA Amplification and Labeling Kit (CapitalBio Co., Ltd, Beijing, China) were applied to amplify and transcribe the RNase R enriched circRNA into fluorescent cRNA with 100–500 ng purified circRNAs. The labelled RNAs were hybridized onto the Human CircRNA Array v2.0. Array hybridization was performed in an Agilent Hybridization Oven overnight at a rotation speed of 20 rpm and 42°C (0.2% SDS, 2× SSC at 42°C for 5 min, followed by 0.2× SSC at 37°C for 5 min). The signals were scanned using the Agilent G2565CA Microarray Scanner, and array images were analysed with the Agilent Feature Extraction software (v10.7). The raw data quantile normalization and data analysis were analysed with Agilent GeneSpring software.

RNA extraction and quantitative real-time PCR (qRT-PCR)

Total RNA was isolated and extracted from human GC tissues and cells using TRIzol Reagent (Takara, #9108, China). The treated RNA was reverse transcribed into the first-strand cDNA by a PrimeScript RT Reagent Kit (Takara, #RR037A) and random primers following the Kit's protocols. The circFGD4 primers designed across the circularization site were designed by Geneseed (Guangzhou, China). All primers (GAPDH, circFGD4, FGD4, APC, Ki-67, PCNA, E-cadherin, and Vimentin; or miR-532-3p and U6) were designed and synthesized by Sangon Biotech (Shanghai, China) or Ribobio (Guangzhou, China), and the primer sequences used are shown in Table 2. The expression of circFGD4, miR-532-3p, and related mRNA in GC tissues and cells was quantified by qRT-PCR using TB Green Premix Ex Taq (Takara, #RR820A). GADPH and U6 were employed as mRNA and miRNA endogenous controls, and the $2^{-\Delta\Delta Ct}$ formula was conducted to analyse the relative expression levels. The PCR products were investigated using 2% agarose gel electrophoresis. The bands were separated by electrophoresis at 120 V for 20 min and were examined by UV irradiation. Then, the PCR products were further identified through Sanger sequencing by Sangon Biotech.

Table 1 Correlations between the proportion of circFGD4 and clinicopathological features in 51 GC patients

Characteristics	No. of patients	circFGD4		*P* value
		Low	High	
All cases	51	35	16	
Age				
≤65	35	25	10	0.524
>65	16	10	6	
Gender				
Male	40	29	11	0.256
Female	11	6	5	
Tumour size (cm)				
≤5	26	15	11	0.086
>5	25	20	5	
Differentiation grade				
Well-moderate	27	15	12	0.033*
Poor-differentiation	24	20	4	
T stage				
T1-T2	11	6	5	0.256
T3-T4	40	29	11	
Lymph node status				
Negative	27	15	12	0.040*
Positive	24	20	4	
Distant metastasis				
M0	46	31	15	0.495
M1	5	4	1	
TNM stage				
I-II	28	20	8	0.634
III-IV	23	15	8	

The median circFGD4 expression score (0.50) was defined as the cut-off value for dividing all GC patients into high- and low-expression groups.
*$P<0.05$.

Table 2 Primers, Probes, and siRNA information

Primers/Probes	Sequence
GAPDH-F	5′-CTTTGGTATCGTGGAAGGACTC-3′
GAPDH-R	5′-GTAGAGGCAGGGATGATGTTCT-3′
circFGD4-F	5′-GAACGCTACCTTTTCTTAAAAC-3′
circFGD4-R	5′-AGGCAATTTCCTTAGATAGTC-3′
FGD4-F	5′-TCTCATCAGTCGCTTTGAAGGA-3′
FGD4-R	5′-GGGTTCTAGGAGCATTTAGGTTC-3′
APC-F	5′-AAAATGTCCCTCCGTTCTTATGG-3′
APC-R	5′-CTGAAGTTGAGCGTAATACCAGT-3′
Ki-67-F	5′-CAGACATCAGGAGAGACTACAC-3′
Ki-67-R	5′-GTTAGACTTGCTGCTGAGTCTA-3′
PCNA F	5′-TAATTTCCTGTGCAAAAGACGG-3′
PCNA R	5′-AAGAAGTTCAGGTACCTCAGTG-3′
E-cadherin F	5′-AGTCACTGACACCAACGATAAT-3′
E-cadherin R	5′-ATCGTTGTTCACTGGATTTGTG-3′
Vimentin F	5′-GGACCAGCTAACCAACGACA-3′
Vimentin R	5′-AAGGTCAAGACGTGCCAGAG-3′
siRNA1-circFGD4	5′-ACGCTACCTTTTCTTAAAACA-3′
	5′-ATAACCGTCAACTATTCCTAT-3′
siRNA2-circFGD4	5′-CGCTACCTTTTCTTAAAACAG-3′
	5′-ACTCGATACGATAATCTTCTC-3′
siRNA3-circFGD4	5′-TACCTTTTCTTAAAACAGAAA-3′
	5′-ATTAACAATACGTTCATACTA-3′
FISH-circFGD4 probe	5′-AGATTTTCTGTTTTAAGAAAAGGTAGCGTT-3′
FISH-miR-532-3p probe	5′-TGCAAGCCTTGGGTGTGGGAGG-3′
Pull down-circFGD4 probe	5′-CTCCCACAGATTTTCTGTTTTAAGAAAAGGTAGCGTTCTT-3′

Clinical Science (2020) **134** 1821–1839
https://doi.org/10.1042/CS20191043

Cell culture and treatments

Human GC cell lines (MKN28, AGS, SGC7901, MKN45, MGC803, and BGC823) were purchased from the Type Culture Collection of the Chinese Academy of Sciences (Beijing, China). The human embryonic kidney cell line (HEK-293T) and the normal gastric mucosal epithelial cell line (GES-1) were donated by the Molecular Tumor and Epigenetics Laboratory from the First Affiliated Hospital of Chongqing Medical University. All cells were cultured in DMEM or RPMI 1640 medium (Gibco, Carlsbad, U.S.A.) supplemented with 10% foetal bovine serum (FBS, Gibco, Grand Island, U.S.A.) and stored in a humidified atmosphere of 5% CO_2 at 37°C. For cell treatments, 2 μg of total RNA was incubated for 30 min at 37°C using 3 U/μg of Ribonuclease R (RNase R; Epicentre Technologies, U.S.A.). Next, GC cells were treated with 2 μg/ml Actinomycin D (Sigma-Aldrich, USA) for 0, 6, 12, 18, and 24 h, respectively. Relative RNA levels of circFGD4 and parental gene FGD4 were performed by qRT-PCR and normalized to the values measured in the 0 h group.

circRNA vector construction and transfection

To construct circFGD4-overexpressing vector, a 345 bp cDNA of circFGD4 was cloned into the pHBLV-CMV-crRNA-EF1-T2A lentiviral or plasmid vector purchased from Hanbio Biotech (Shanghai, China). To knockdown circFGD4, three individual circFGD4 siRNAs (siRNA1, siRNA2, and siRNA3) targeting the back-splice junction site of circFGD4 and a siRNA negative control (si-NC) were designed. Based on qRT-PCR results, siRNA1 was significantly the most effective siRNA and was used to construct the siRNA plasmid, named shRNA1, and si-NC was used to construct the sh-NC plasmid (GenePharma). The miRNA negative control (miR-NC), miR-532-3p mimics, and miR-532-3p inhibitors were designed and synthesized by Ribobio (Guangzhou, China). The nucleotide sequences are listed in Table 2. All oligonucleotides and overexpressing- or knockdown-plasmids were transfected into GC cell lines using Lipofectamine 2000 Reagent (Invitrogen, Carlsbad, U.S.A.). After transfection for 48–72 h, cells were harvested for further experiments.

Cell Counting Kit-8 (CCK-8) and colony formation assays

GC cell viability detection was employed using the CCK-8 Kit (Dojindo, Kumamoto, Japan) following the manuals from the manufacturer. Briefly, about 10^3 transfected GC cells were seeded into 96-well plates, and 10 μl CCK-8 was added to each well for 3 h at 37°C with 5% CO_2. The optical density value was evaluated in 0, 24, 48, 72, and 96 h at 450 nm using a Microplate Reader. Next, approximately 200 transfected GC cells were seeded into 24-well plates and cultured for 14 days regarding colony formation assay. The colonies were fixed with 4% paraformaldehyde and stained using 0.1% Crystal Violet, and visible colonies were photographed and manually counted.

Ethynyl deoxyuridine (EdU) staining assay

Proliferating cells were assessed using an EdU Labeling/Detection Kit (RiboBio, China) following the Kit's instructions. The treated GC cells were seeded in 96-well plates at 1×10^4 cells per well and cultured to the logarithmic growth phase. The abovementioned GC cells were treated with EdU solution and Apollo staining reaction solution. Cell nuclei were stained with Hoechst 33342 reaction solution. The percentage of EdU positive cells was evaluated using a confocal laser scanning microscopy (LSM800, Carl Zeiss AG, Germany), and images were obtained and counted.

Transwell migration and wound healing assays

For cell transwell assay, the serum-free medium containing 4×10^4 transfected cells was placed into the 24-well transwell chambers (8 μm pore size, Corning Costar, U.S.A.), and complete medium containing 10% FBS was added to the lower chambers. After incubation for 24 h, the migratory cells at the lower surfaces of chambers were fixed using methanol and stained using 0.1% Crystal Violet solution, and next photographed. The transfected target cells were evenly plated into a six-well plate, and the cells were cultured to 90% confluency after 24 h for wound healing assays. A 10 μl sterile tip perpendicular to a six-well plate was used for scratches and photographed at 0 h. Then, the cells were cultured in the serum-free medium, and images were obtained after 24 h.

RNA fluorescence *in situ* hybridization (FISH)

RNA FISH probes for the circFGD4 and miR-532-3p sequences were designed and synthesized by GenePharma. GC cells were seeded and fixed in 24-well plates containing climbing pieces. Cy3 probes were specific to circFGD4, and FAM probes were specific to miR-532-3p. 4′6-Diamidino-2-phenylindole (DAPI; Life Technologies, Carlsbad, U.S.A.) was applied to label cell nuclei. The probe signals were measured by using Fluorescent In Situ Hybridization

Kit (GenePharma) following the Kit' s guidelines. The fluorescent signals were determined by using a confocal microscope (LSM800, Carl Zeiss AG, Germany). The sequences of circFDG4 and miR-532-3p probes are listed in Table 2.

Immunofluorescence (IF)

Briefly, GC cells were plated onto 24-well plates with climbing pieces and transfected with the circFGD4 overexpression plasmid, the shRNA1 plasmid, and some of the cells were also cotransfected with miR-NC or miR-532-3p mimics + circFGD4 overexpression plasmid and miR-NC or miR-532-3p inhibitors + circFGD4 shRNA1 plasmid separately for 48 h. The cells were incubated with APC, E-cadherin, and Vimentin (Abcam, Burlingame, U.S.A.) primary antibodies at 4°C overnight, followed by incubating the corresponding fluorescent secondary antibodies. DAPI was used to stain the cellular nuclei, and all transfected cells were detected and observed using a confocal microscope (LSM800, Carl Zeiss AG, Germany).

RNA immunoprecipitation (RIP) assay

RIP-binding protein immunoprecipitation assay was carried out in AGS cells by a Magna RIP RNA-binding protein Immunoprecipitation Kit (Millipore, Billerica, U.S.A.) and human anti-Argonaute2 antibody (AGO2, Cell Signaling Technology, U.S.A.) following the manufacturer's protocols. Briefly, 1×10^7 AGS cells stably transfected with miR-NC or miR-532-3p mimics were washed by ice-cold PBS and lysed in an equal volume of RIP lysis buffer. The cell lysates were incubated with negative control anti-AGO2 antibody or rabbit IgG-coated magnetic beads and rotated at 4°C overnight. After treating the cell lysates with proteinase K buffer, the RNA fraction was purified and extracted to detect the AOG2 protein, circFGD4, and miR-532-3p.

Biotin-coupled probe pull-down assay

For circFGD4 pulled down miRNAs, AGS cells ($> 1 \times 10^7$) stably expressed circFGD4 were harvested, lysed with lysis buffer, and sonicated. To generate probe coated beads, the biotinylated circFGD4 probe (control: oligo probe) was incubated with streptavidin magnetic beads (Invitrogen, U.S.A.) at room temperature for 2 h. The cell lysates were incubated using the circFGD4 probe at 4°C overnight. Next, the treated beads were washed, and the RNA complexes were eluted, purified and extracted with TRIzol (Takara) for qRT-PCR. Biotinylated probe sequence of circFGD4 was designed (GenePharma, China) and is showed in Table 2.

Dual-luciferase reporter assay

Luciferase reporter plasmids (pGL3- wild-type (WT) or -mutant-type (MUT) circFGD4 fragment and pGL3- WT or -MUT APC fragment) were designed and synthesized by GenePharma (China). HEK-293T cells grown in a 96-well plate were cotransfected with corresponding plasmids containing pGL3- WT or -MUT circFGD4 and APC fragment and miR-532-3p mimics or control miR-NC using Lipofectamine 2000 (Invitrogen, U.S.A.). After culturing for 48 h, the luciferase values based on firefly and Renilla were detected by the Dual-Luciferase® Reporter Assay System (Promega, Madison, U.S.A.). Relative luciferase activity was calculated as the ratio between the firefly and Renilla luciferase values for each sample.

TOP/Flash and FOP/Flash reporter assay

HEK-293T and GC cells were cultured for 12–24 h and then cotransfected with the miR-NC, miR-532-3p mimics, miR-532-3p inhibitors, miR-532-3p mimics + circFGD4 overexpression plasmid, and miR-532-3p inhibitors + circFGD4 shRNA1 plasmid respectively combined with TOPFlash, FOPFlash and Renilla luciferase plasmid (Addgene, Cambridge, U.S.A.). After 48 h of transfection, cells were lysed by using lysis buffer, and then stimulated with 20 mM LiCl- or 15% Wnt3A- conditioned medium for 6 h. The luciferase activities were detected with Luciferase Reporter Gene Assay Kit (Promega) [13]. All luciferase activities were normalized to Renilla luciferase activity and are presented as relative luciferase activities.

Western blot analysis

Proteins extraction from GC cells were conducted using RIPA buffer containing complete protease and phosphatase inhibitors for 30 min on ice and sonicated. Also, Nuclear and Cytoplasmic Protein Extraction Kits (Beyotime, China) were utilized to isolate and extract the cytoplasmic and nuclear proteins separately. The equal quantities of protein extractions were separated on 10% SDS-PAGE and then transferred onto polyvinylidene fluoride (PVDF) membranes (Bio-Rad, CA, U.S.A.). These membranes were blocked with quick blocking solution and incubated with the specific

Clinical Science (2020) **134** 1821–1839
https://doi.org/10.1042/CS20191043

primary antibodies against PCNA, Ki-67, Vimentin, E-cadherin, N-cadherin, APC, β-catenin, β-actin, GAPDH, and Lamin B1 (Abcam) at 4°C overnight. The membranes were washed with TBST buffer and incubated with horseradish peroxidase (HRP)-conjugated secondary antibodies at room temperature for 2 h. After washing, samples were visualized using the enhanced chemiluminescence (RCL) reagent (Bio-Rad, U.S.A.).

Animal experiments

Four-week-old BALB/c female nude mice were purchased from the National Laboratory Animal Centre (Shanghai, China). Approximately 5×10^6 MGC803 cells transfected with lentivirus overexpressing circFGD4 and negative control vector (NC) were administrated into the axilla of each mouse by subcutaneous injections (five mice per group). Nude mice were killed by intraperitoneal injection of a 3-fold anesthetic dose of sodium pentobarbital (150–200 mg/kg) after 4 weeks, followed by the xenograft tumours were harvested and calculated as $0.5 \times \text{length} \times (\text{width})^2$, and then used for qRT-PCR and IHC assays. For the metastasis model, 1×10^7 transfected MGC803 cells in 50 μl of PBS were injected into BALB/c nude mouse (4 weeks old) via their tail veins, including the blank group, the NC group, and the circFGD4 overexpression group. After 4 weeks of feeding, the mouse was killed and examined the number and size of macroscopically visible lung metastatic nodules in nude mice. The images of metastatic nodules in mouse lungs were captured, and the metastatic nodules were used for qRT-PCR. All animal protocols were under the approval of the Animal Ethics Committee of Chongqing Medical University, and conducted at the Animal Experimental Centre of Chongqing Medical University, and carried out following the National Institute of Health Guide for the Care and Use of Laboratory Animals.

Immunohistochemical (IHC) staining

Briefly, mice xenograft tumours embedded in paraffin, sectioned into 4 μm thick, placed on glass slides and stained with IHC. After the sections were deparaffinized, rehydrated, and antigen retrieval, the sections were incubated at 4°C overnight with primary antibodies against APC, Ki-67, PCNA, E-cadherin, and Vimentin (Abcam; 1:50 dilution). Next day, after incubation with HRP-conjugated goat anti-rabbit IgG at 25°C for 1 h, then the sections were stained with diaminoaniline (DAB) and counterstained with haematoxylin. Lastly, the sections were covered with coverslips for a fluorescence microscope (Axio Imager A2, Carl Zeiss AG, Germany).

Statistical analysis

The graph plots and statistics were carried out using GraphPad Prism 8.2.1 software. P-value < 0.05 was taken as statistically significant. Statistical significance was evaluated by Student's t-test or analysis of variance followed by multiple comparison tests. The association of circFGD4 levels with the GC patients' clinic-pathological variables was analysed by the chi-square(χ^2) test or Fisher's exact test. Overall survival (OS) curves were performed with the Kaplan–Meier method and analysed by the log-rank test. The correlation between circFGD4 and miR-532-3p expression or circFGD4 and FGD4 expression was analysed by Pearson's correlation coefficient analysis. All results were conducted at least three independent experiments.

Results

circFGD4 was lowly expressed in GC tissues and correlated with the progression and prognosis of GC patients

To investigate the circRNA expression profile in GC tissues, we characterized circRNA transcripts in GC tissues by analysing databases from the GEO database (GSE100170 and GSE131414) and our circRNA microarray (Figure 1A). In our circRNA microarray, the clustered heat map showed that a total of 3988 dysregulated circRNAs with 2-fold change ($P<0.05$) were screened and identified between GC tissues and paired noncancerous tissues (Figure 1B). By excluding low-abundance circRNAs (scores are too small) from the circBase website [14], two circRNAs (hsa_circ_0000390 and hsa_circ_0007315) significantly differentially expressed in circRNA microarray were verified by qRT-PCR analysis for their expression levels in GC tissues. We found that the relatively higher hsa_circ_0000390 expression levels than the expression levels of hsa_circ_0007315 in GC tissues (Figure 1C). The qRT-PCR analysis also confirmed that the expression of hsa_circ_0000390 was lower expressed in six GC cell lines (MKN28, SGC7901, AGS, MKN45, MGC803, and BGC823) than in GES-1 cells (Figure 1D). Therefore, hsa_circ_0000390 was selected as the studied molecule.

Under RNase R treatment, the levels of FGD4 linear forms were significantly reduced, but RNase R could not digest hsa_circ_0000390 in SGC7901 cells (Figure 1E). Actinomycin D is a transcriptional inhibitor that has been used to treat SGC7901 cells. The results validated that the half-life of hsa_circ_0000390 was more than 24 h, while the

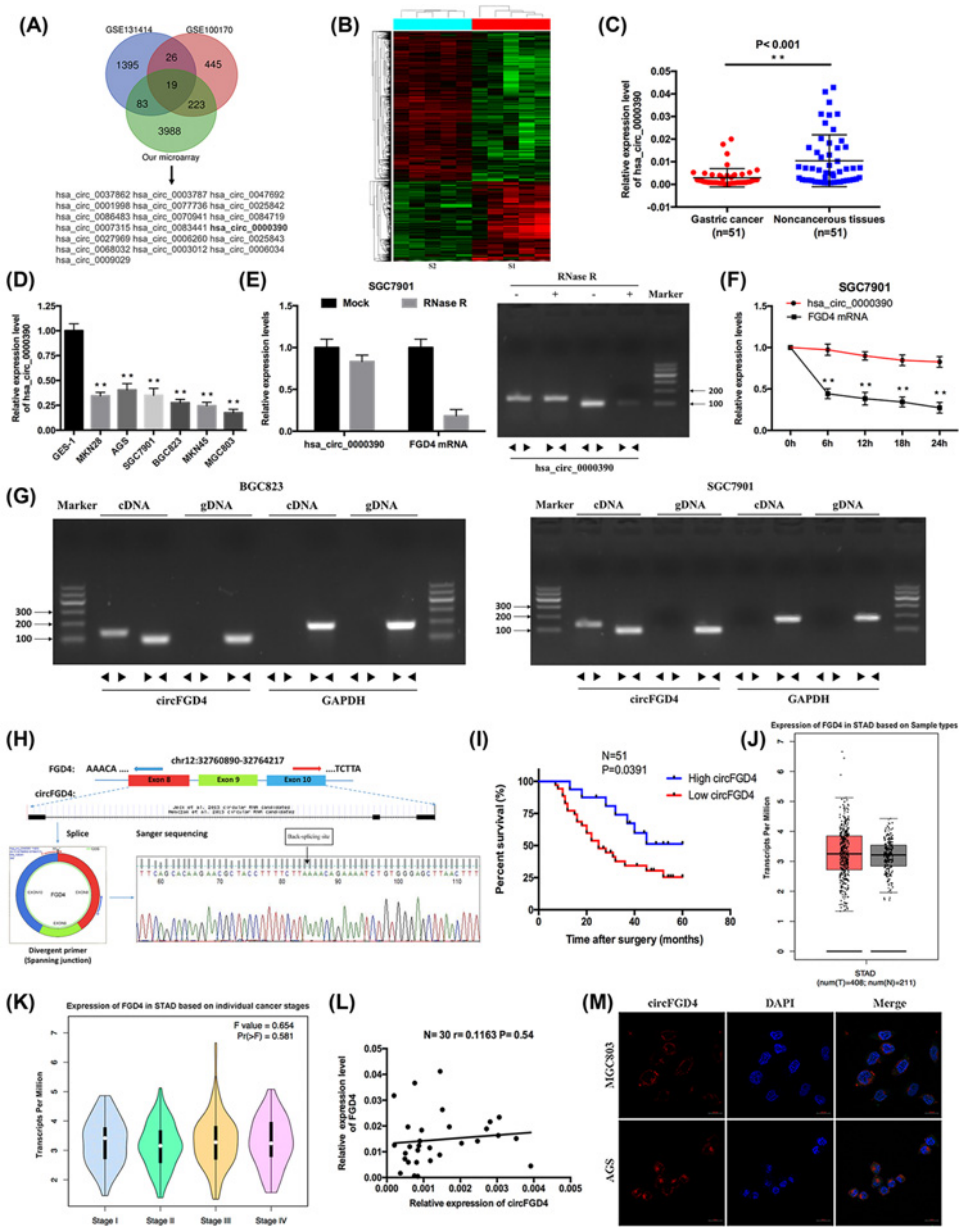

Figure 1. circFGD4 was down-regulated in GC and associated with the progression and poor prognosis of GC patients

(**A**) Schematic illustration exhibiting the overlapping of circRNAs predicted by GSE100170 and GSE131414 and our circRNA microarray (CapitalBio Technology Co., Ltd). (**B**) Clustered heat map displaying the tissue-specific circRNAs in five paired human GC tissues and noncancerous tissues. GC tissues: S1; Paired noncancerous tissues: S2. (**C**) Relative expression level of circFGD4 was detected by qRT-PCR in 51 paired GC tissues and noncancerous tissues. (**D**) Relative expression level of circFGD4 was examined by qRT-PCR in six GC cell lines and GES-1 cells. (**E**) The expression of circFGD4 and FGD4 RNA was validated by qRT-PCR after treatment with RNase R in SGC7901 cells. (**F**) The expression of circFGD4 and FGD4 RNA was determined by qRT-PCR after treatment with Actinomycin D at the indicated time points in SGC7901 cells. (**G**) qRT-PCR validated the existence of circFGD4 in BGC823 and SGC7901 cell lines. circFGD4 was amplified by divergent primers in cDNA but not gDNA. (**H**) Schematic representation of circFGD4 formation. The back-splice junction sequence of circFGD4 was validated by Sanger sequencing. (**I**) Kaplan–Meier plotter analysis of the correlation of circFGD4 expression level with the overall survival of GC patients. (**J**) TCGA database analysis of FGD4 mRNA levels in human GC normal tissues (n=211) and tumour tissues (n=408). (**K**) Violin plot of relative abundance of FGD4 mRNA levels in different stages of GC tissues from the TCGA database. The white dot represents the median. (**L**) Correlation analysis of circFGD4 levels with FGD4 mRNA levels in 30 GC tissues. (**M**) Confocal FISH was performed to observe the cellular location of circFGD4 in MGC803 and AGS cells (values are shown as the mean ± standard error of the mean based on three independent experiments; $^{*}P<0.05$, $^{**}P<0.01$).

Clinical Science (2020) **134** 1821–1839
https://doi.org/10.1042/CS20191043

half-life of linear FGD4 mRNA was lower than 6 h by qRT-PCR analysis, indicating hsa_circ_0000390 is highly stable in SGC7901 cells (Figure 1F). Bioinformatics analysis showed that hsa_circ_0000390 was located on chromosome chr12:32760890-32764217, was 345 bp long, and was formed from exons 8, 9 and 10 of FGD4; thus, we termed it circFGD4. To more rigorously validate the result of back-splicing, a convergent primer for FGD4 mRNA and a special divergent primer for the amplification of circFGD4 were designed. Extraction of cDNA and gDNA from BGC823 and SGC7901 cells for gel electrophoresis detection, and results displayed that circFGD4 could be detected only in cDNA, but no products in gDNA (Figure 1G). Also, the back-splicing junction of circFGD4 was further confirmed in PCR products by Sanger sequencing (Figure 1H). The expression level of circFGD4 was reduced in GC patients with poor tumour differentiation (P=0.033) and lymphatic metastasis (P=0.04) (Table 1). More important, low circFGD4 expression had a significantly poor prognosis of GC patients compared to patients with high circFGD4 expression (P=0.0391; Figure 1I).

To investigate whether circFGD4 levels correlate with linear FGD4 mRNA levels in GC tissues, the data from the TCGA database indicated that linear FGD4 mRNA levels had no significant difference between 408 GC tissues and 211 paired noncancerous tissues (Figure 1J). Also, there was no statistical change in the expression level of linear FGD4 mRNA at different GC stages (Figure 1K). The correlation analysis displayed that circFGD4 levels were not specifically associated with FGD4 mRNA levels in 30 GC tissues (Figure 1L). Additionally, RNA FISH assays displayed that circFGD4 was predominately localized in the cytoplasm of GC cells (Figure 1M). Together, these results suggested that lower circFGD4 expression was generally observed in GC tissues and cells and correlated with a worse prognosis in GC patients.

Knockdown of circFGD4 promoted GC cell viability, colony formation, DNA synthesis, migration, and induced EMT

Given the down-regulation of circFGD4 in GC tissues and cell lines, the loss-of-function assays were applied to verify whether circFGD4 could affect the viability, colony formation, and migration of GC cells. We analysed the shRNA1 sequence of circFGD4 at back-splice junctions and designed the circFGD4-shRNA1 plasmid accordingly (Figure 2A). After shRNA1 was transfected into AGS and BGC823 cell lines for 48 h, the silencing efficiency of circFGD4 was detected by qRT-PCR (Figure 2B). CCK-8 and colony formation assays indicated that knockdown of circFGD4 expression promoted the cell viability and colony-forming abilities of AGS and BGC823 cells (Figure 2C,D). EdU incorporation assays indicated that DNA synthesis in AGS and BGC823 cells was accelerated after knockdown of circFGD4 compared with the sh-NC vector (Figure 2E). Transwell assays demonstrated that the cell migration of both AGS and BGC823 cells were prominently promoted by the circFGD4 shRNA1 transfection, which was consistent with the wound healing assays (Figure 2F,G). Additionally, IF assays indicated that the knocking down of circFGD4 increased vimentin expression and decreased E-cadherin expression in AGS cells (Figure 2H). These findings suggested that the silencing of circFGD4 expression promoted GC cell proliferation, migration, and induced EMT *in vitro*.

Enforced circFGD4 suppressed the growth, colony formation, migration and EMT of GC cells

Based on circFGD4 knockdown experiments, we investigated the potential functional role of circFGD4 through gain-of-function experiments in GC cells. qRT-PCR assays indicated that overexpression efficiency of circFGD4 after the transfection was efficient in MGC803 and SGC7901 (Figure 3A). The extraction and sequencing of RNA obtained from cells overexpressing circFGD4 confirmed that the overexpressed circFGD4 was circular rather than linear. A series of proliferation-related experiments indicated that the viability, colony formation, and DNA synthesis abilities of MGC803 and SGC7901 cells were significantly decreased in the circFGD4 overexpression group compared with the negative control (NC) group (Figure 3B–D). Transwell migration assays demonstrated that the migrated cells were significantly decreased when circFGD4 was overexpressed at MGC803 and SGC7901 cells (Figure 3E). Also, IF assays demonstrated that the gain of circFGD4 condensed and aggregated the morphology of MGC803 cells without dispersion, followed by changes in EMT markers, including an increased E-cadherin expression and decreased vimentin expression (Figure 3F). In contrast, EMT changes after enforced circFGD4 were opposite to the effect of knocking down circFGD4 in GC cells. The data confirmed that circFGD4 was a tumour suppressor of GC progression and metastasis *in vitro*.

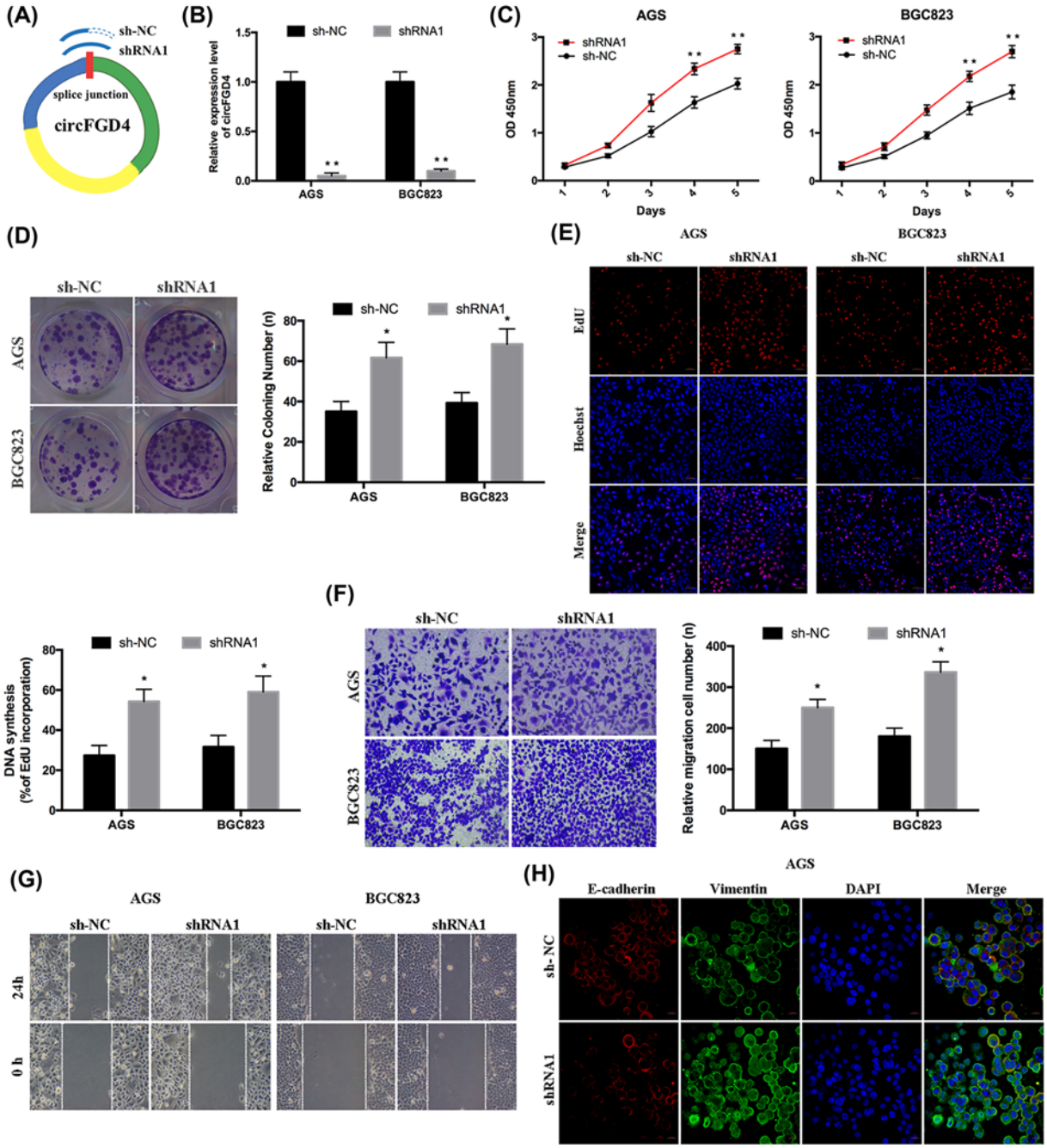

Figure 2. Knockdown of circFGD4 promoted the viability, migration, and EMT of GC cells

(**A**) Schematic representation of shRNA1 and sh-NC designed to target circFGD4 at the back-splice junctions. (**B**) Relative expression of circFGD4 was detected by qRT-PCR in AGS and BGC823 cells transfected with shRNA1 targeting circFGD4. (**C** and **D**) Cell proliferation abilities were detected by CCK-8 and colony formation assays after the transfection of shRNA1 or sh-NC in AGS and BGC823 cells. (**E**) DNA synthesis was observed by EdU assays after the transfection of shRNA1 or sh-NC in AGS and BGC823 cells. (**F**) Cell migration abilities were determined by transwell assays after the transfection of shRNA1 or sh-NC in AGS and BGC823 cells. (**G**) Cell migration capacities were detected by wound healing assays after the transfection of shRNA1 or sh-NC in AGS and BGC823 cells. (**H**) Representative images of the expression levels of E-cadherin (red) and vimentin (green) in AGS cells were assessed by IF after transfection. Nuclei were counterstained with DAPI (blue) (values are shown as the mean ± standard error of the mean based on three independent experiments; $^{*}P<0.05$, $^{**}P<0.01$).

Clinical Science (2020) **134** 1821–1839
https://doi.org/10.1042/CS20191043

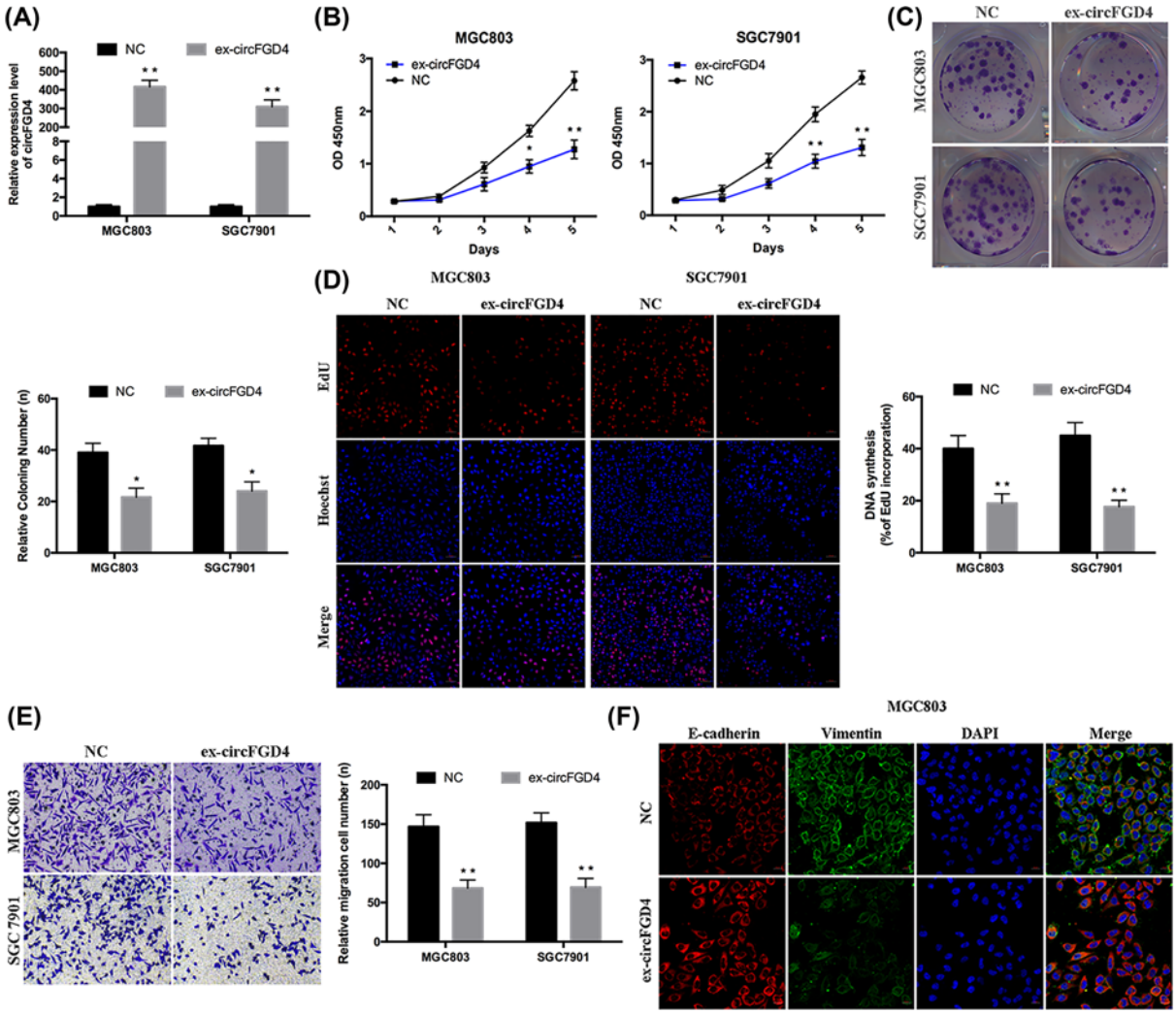

Figure 3. Overexpression of circFGD4 inhibited GC cell growth, migration, and EMT *in vitro*

(**A**) Relative expression of circFGD4 was confirmed by qRT-PCR in MGC803 and SGC7901 cells overexpressing circFGD4. (**B–D**) Cell viability assays of MGC803 and SGC7901 cells overexpressing circFGD4 measured by CCK-8 assays (B), colony formation assays (C), and EdU assays (D). (**E**) Transwell analysis of cell migration potential after transfection of MGC803 and SGC7901 cells with circFGD4 overexpression plasmid or NC plasmid. (**F**) Representative images of IF micrographs showing the subcellular localization and expression of E-cadherin (red) and vimentin (green) in MGC803 cells. Nuclei were counterstained with DAPI (blue) (values are shown as the mean ± standard error of the mean based on three independent experiments; $^{*}P<0.05$, $^{**}P<0.01$).

circFGD4 directly interacted with miR-532-3p in GC

To elucidate whether circFGD4 exerts anticancer effects through sponge-binding miRNAs, we first predicted a total of 55 potential conjugated miRNAs using online prediction tools (Circinteractome [15], Circbank [16], RegRNA [17], CSCD [18]; Figure 4A). The qRT-PCR results indicated that the expression levels of hsa-miR-32-5p, hsa-miR-150-5p, has-miR-532-3p, and hsa-miR-629-3p in 20 GC tissues compared with their paired noncancerous tissues (Figure 4B). Further validation revealed that miR-532-3p expression was higher in GC tissues than in noncancerous tissues (Figure 4C). FISH assays were used, and the results indicated that circFGD4 and miR-532-3p were colocalized in the cytoplasm of MGC803 and AGS cells (Figure 4D). Subsequently, the circFGD4-WT and circFGD4-MUT miR-532-3p binding sites were subcloned into the dual-luciferase reporters (Figure 4E). The results revealed that miR-532-3p mimics reduced the luciferase activity of circFGD4-WT, but had no effects on that of circFGD4-MUT in HEK-293T cells (Figure 4F). Additionally, an anti-AGO2 RIP assay revealed that endogenous circFGD4 was pulled down by anti-AGO2 antibodies and was mainly enriched in the AGO2 group than the IgG control group (Figure 4G), and both

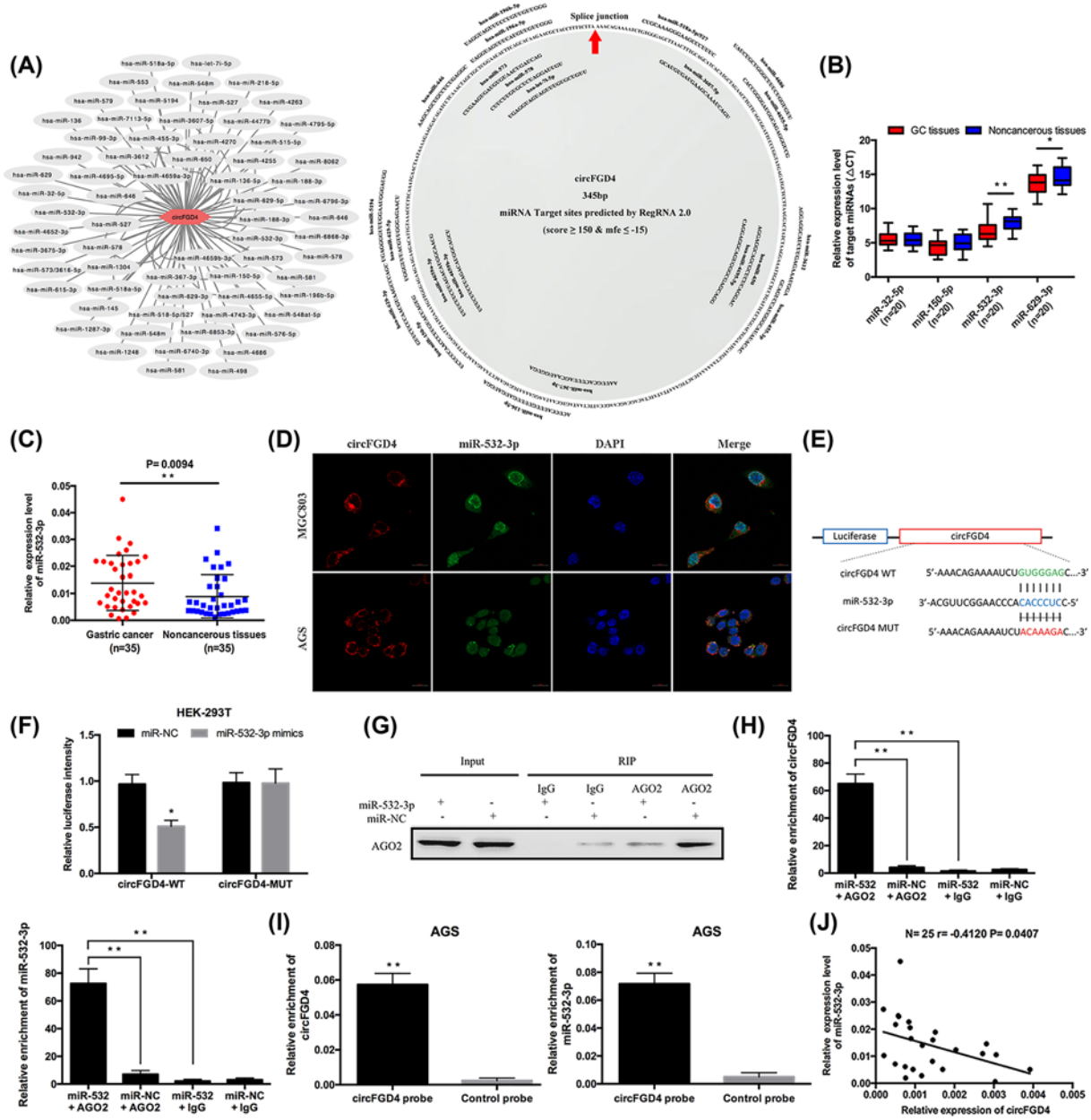

Figure 4. circFGD4 directly interacted with miR-532-3p in GC

(**A**) A magnified network comprising circFGD4 and its target miRNAs was presented. The binding sites of miRNAs and circFGD4 were predicted by RegRNA 2.0. (**B**) The expression levels of four candidate miRNAs were confirmed by qRT-PCR in 20 paired GC cancer tissues and noncancerous tissues. (**C**) Relative expression levels of miR-532-3p were up-regulated in GC tissues compared with their paired noncancerous tissues by qRT-PCR analysis. (**D**) FISH assays were performed to observe the cellular colocalization of circFGD4 (red) and miR-532-3p (green) in MGC803 and AGS cells. (**E**) Schematic illustration of circFGD4-WT and circFGD4-MUT luciferase reporter vectors. (**F**) Relative luciferase activities were detected in HEK-293T cells after cotransfection with circFGD4-WT or circFGD4-MUT and miR-532-3p mimics or miR-NC, respectively. (**G** and **H**) Anti-AGO2 RIP was performed in AGS cells after transfection with miR-532-3p mimics or miR-NC, followed by Western blot and qRT-PCR to detect AGO2 protein, and circFGD4 and miR-532-3p, respectively. (**I**) RNA pull-down assays were performed in AGS cells, followed by qRT-PCR to detect the enrichment of circFGD4 and miR-532-3p. (**J**) Pearson correlation analysis of circFGD4 and miR-532-3p expression levels in 25 GC tissues (values are shown as the mean ± standard error of the mean based on three independent experiments; $^{*}P<0.05$, $^{**}P<0.01$).

Clinical Science (2020) **134** 1821–1839
https://doi.org/10.1042/CS20191043

circFGD4 and miR-532-3p were also predominantly enriched in AGS cells which were transfected with miR-532-3p mimics (Figure 4H). Next, by using circFGD4 pull-down experiments, we purified circFGD4-associated RNAs and analysed candidate miRNAs in the complex. The specific enrichment of miR-532-3p that was abundantly detected by qRT-qPCR in the circFGD4 probe and was markedly higher than the miR-NC group in AGS cells (Figure 4I). Furthermore, the expression of miR-532-3p was reversely correlated with that of circFGD4 in GC tissues ($r = -0.412$, P=0.0407; Figure 4J). These results demonstrated that circFGD4 acted as an effective sponge of miR-532-3p in GC.

circFGD4 suppressed GC cell growth, migration, and EMT by sponging miR-532-3p and regulated target gene APC of miR-532-3p

We further validated the functional roles of circFGD4 and miR-532-3p in GC cells by rescue assays such as CCK-8, colony formation, and Transwell migration assays. The levels of miR-532-3p were up- or down-regulated by qRT-PCR after the transfection of MGC803 or AGS cells with miR-532-3p mimics or inhibitors, respectively (Figure 5A). CCK-8 assays indicated that circFGD4 inhibited MGC803 cell proliferation and that miR-532-3p mimics attenuated this inhibition. Also, the silencing of circFGD4 promoted AGS cell growth, and the miR-532-3p inhibitors relieved this promotion (Figure 5B). Western blotting indicated that circFGD4 decreased the PCNA and Ki-67 expression at protein levels, and miR-532-3p mimics inversed this tendency (Figure 5C). Colony formation assays showed similar proliferation effects (Figure 5D). Transwell assays validated that circFGD4 reduced MGC803 cell migration and that the miR-532-3p mimics attenuated this suppression. Silencing of circFGD4 increased AGS cell migration, and miR-532-3p inhibitors weakened this acceleration (Figure 5E). Western blotting demonstrated that the circFGD4/miR-532-3p axis also regulated the EMT-related markers (such as E-cadherin, N-cadherin, and vimentin) in GC cells (Figure 5F). These results indicated that circFGD4 inhibited GC progression and metastasis by abolishing the oncogenic effect of miR-532-3p.

Based on the combined results of target prediction analyses, we found that circFGD4 and the 3′-UTR of APC shared the same miR-532-3p (miRNA Response Elements) MREs (Figure 5G). Western blotting verified that overexpression or silencing of circFGD4 increased or reduced the expression of APC, respectively. Also, miR-532-3p mimics and inhibitors regulated the expression of the APC mRNA and protein, respectively. Rescue assays further indicated that the up- or down-regulation of APC expression levels transfected with miR-532-3p inhibitors or mimics could be restored by the cotransfection of shRNA1 + miR-532-3p inhibitors or circFGD4 overexpression + miR-532-3p mimics (Figure 5H). Subsequently, full-length APC-WT and APC-MUT (red font as mutant locus) were subcloned into the dual-luciferase reporters (Figure 5I). As expected, the luciferase reporter gene assays demonstrated that cotransfection with miR-532-3p mimics and pGL3-APC-WT vector exhibited reduced luciferase activity, whereas miR-532-3p mimics failed to inhibit the luciferase activity of pGL3-APC-MUT vector in HEK-293T cells (Figure 5J). Additionally, the bioinformatics analysis indicated that GC patients with low APC expression had a poor overall survival compared with those with high APC expression (Figure 5K). IF assays also revealed that circFGD4 significantly controlled the expression of APC via the regulation of miR-532-3p in MGC803 and AGS cells (Figure 5L). All these data indicated that circFGD4 could affect the expression of APC by directly interacted with miR-532-3p in GC.

circFGD4/miR-532-3p axis inhibited GC cell viability, migration and induced EMT via β-catenin signalling in an APC-modulated manner

A multi-database analysis found that multiple mRNAs, including APC, were potential targets of miR-532-3p (Figure 6A). The underlying biological processes of 159 potential target mRNAs of miR-532-3p were predicted by the DAVID v6.8 database, and the results indicated that the downstream genes were preferentially enriched in cell migration and the Wnt/β-catenin pathway (Figure 6B,C). Meanwhile, APC protein, a key negative regulator, contributed to multiple tumours progression by modulating Wnt/β-catenin signalling pathway [19]. Therefore, TOP/Flash and FOP/Flash reporter gene were constructed and performed to detect whether the Wnt/β-catenin pathway was activated in GC cells. TOP/FOP transcriptional activity was enhanced or reduced after the transfection of the knockdown or overexpression of circFGD4 vectors in HEK-293T, MGC803, and AGS cells (Figure 6D,E). Further experiments showed that circFGD4 overexpression with the transfection of MGC803 and AGS cells reversed the increase in TOP/FOP transcriptional activity induced by miR-532-3p mimics (Figure 6F). The knocking down of circFGD4 also reversed the decline in the TOP/FOP transcriptional activity prompted by miR-532-3p inhibitors in MGC803 and AGS cells (Figure 6F). Western blotting indicated that cotransfection of circFGD4 and miR-532-3p in MGC803 and AGS cells could not significantly modulate the total protein of β-catenin; However, β-catenin protein in the nucleus of GC cells displayed distinct changes (Figure 6G). The nuclear/cytoplasmic ratios of β-catenin were significantly increased in shRNA1-transfected AGS cells compared to AGS cells transfected only with miR-532-3p inhibitors, but cotransfection

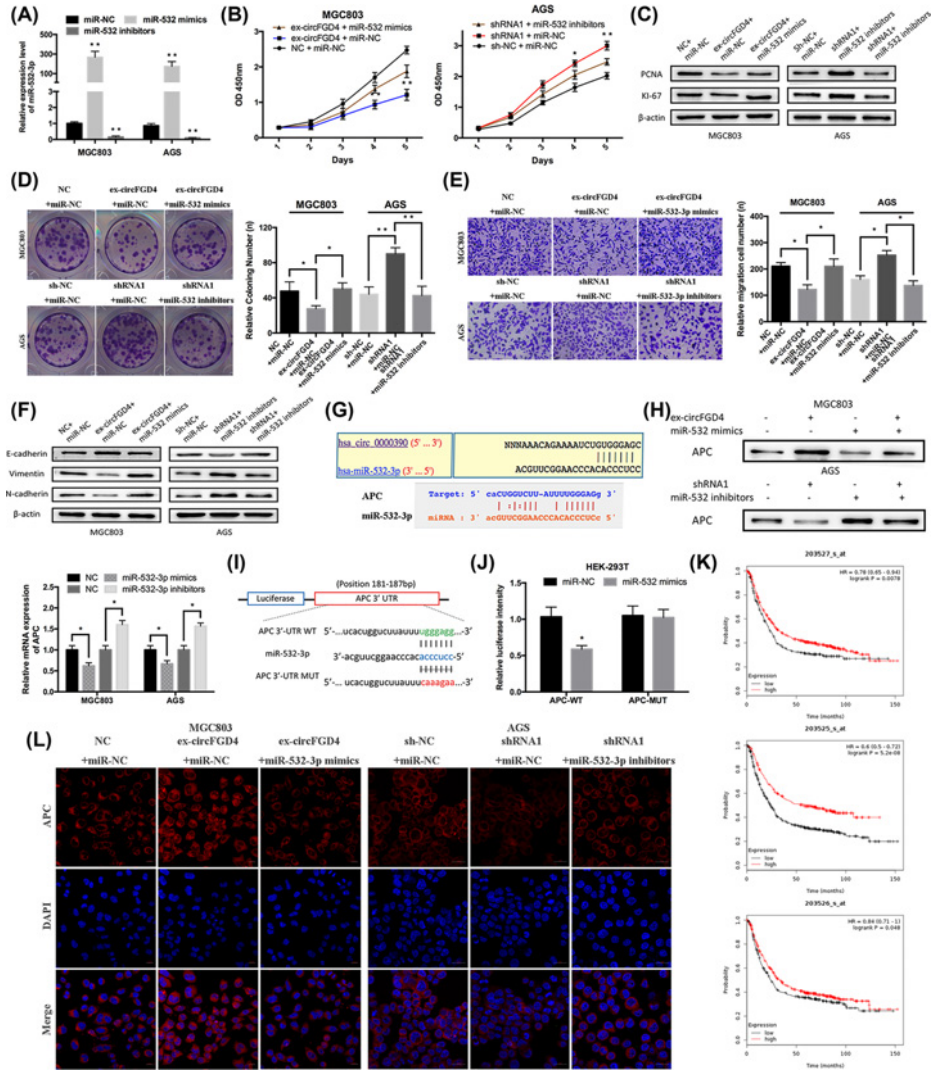

Figure 5. circFGD4 suppressed GC cell growth, migration, and EMT by sponging miR-532-3p and regulated target gene APC of miR-532-3p

(**A**) Relative expression of miR-532-3p in MGC803 and AGS cells transfected with miR-532-3p mimics or inhibitors, respectively. (**B**) CCK-8 assays were performed to assess the proliferation abilities of the transfected MGC803 cells and AGS cells. MGC803 cells were transfected with NC, circFGD4 overexpression vector, circFGD4 overexpression vector and miR-532-3p mimics, respectively. AGS cells were transfected with sh-NC, shRNA1, shRNA1 and miR-532-3p inhibitors, respectively. (**C**) The expression levels of PCNA and Ki-67 were detected by Western blotting in MGC803 and AGS cells cotransfected with the indicated vectors and miR-532-3p mimics or inhibitors, respectively. (**D**) The colony-forming abilities of the transfected MGC803 and AGS cells that were examined by colony formation assays. (**E**) The migration of MGC803 and AGS cells was determined by transwell assays after transfection with the indicated vectors, miR-532-3p mimics or inhibitors, respectively. (**F**) The expression levels of E-cadherin, N-cadherin, and vimentin were validated by Western blotting in MGC803 and AGS cells cotransfected with the indicated vectors and miR-532-3p mimics or inhibitors, respectively. (**G**) Schematic representation of the potential binding sites of circFGD4 to miR-532-3p and miR-532-3p to the 3′ UTR of APC. (**H**) The expression level of APC protein was detected by Western blotting in MGC803 and AGS cells transfection with miR-NC, miR-532-3p mimics or miR-532-3p inhibitors, circFGD4 overexpression vector or shRNA1 vector, and miR-532-3p mimics + circFGD4 overexpression vector or miR-532-3p inhibitors + shRNA1 vector, respectively. (**I**) Schematic representation of APC 3′UTR-WT and APC 3′UTR-MUT luciferase reporter vectors. (**J**) Luciferase reporter assays demonstrated that APC-WT is a direct target of miR-532-3p mimics in HEK-293T cells. (**K**) Kaplan–Meier analysis of overall survival in GC patients with variable expression of three APC probes. (**L**) Relative expression levels of APC were assessed by IF after MGC803 and AGS cells were transfected with circFGD4 overexpression plasmid or shRNA1 silencing plasmid and miR-532-3p mimics or inhibitors, respectively (values are shown as the mean ± standard error of the mean based on three independent experiments; $^{*}P<0.05$, $^{**}P<0.01$).

Clinical Science (2020) **134** 1821–1839
https://doi.org/10.1042/CS20191043

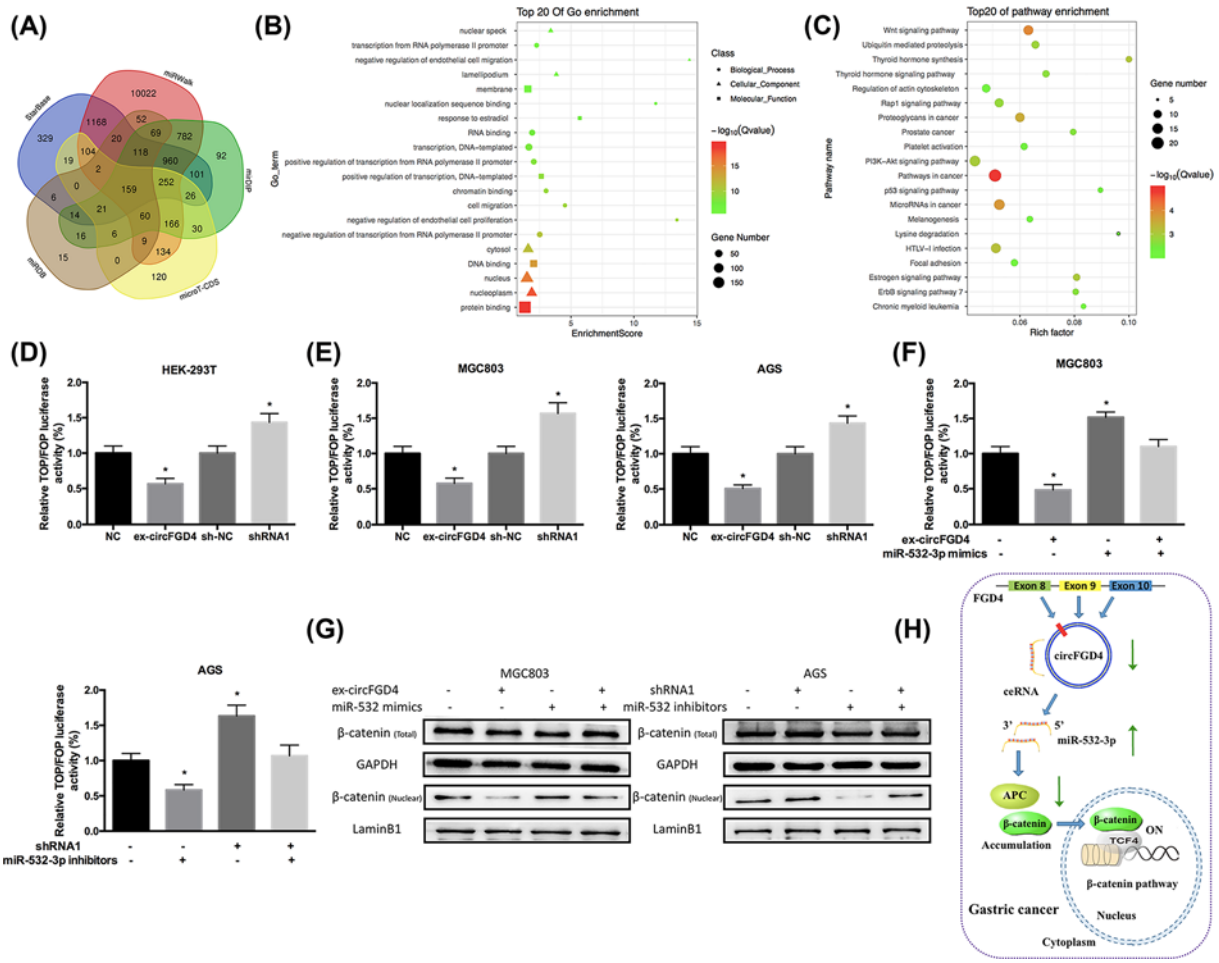

Figure 6. circFGD4/miR-532-3p axis suppressed GC cell viability, migration and EMT via β-catenin signalling in an APC-modulated manner

(**A**) Schematic diagram showing the 159 commonly differentially expressed mRNA targets of miR-532-3p obtained from five publicly available profile databases (StarBase, miRWalk, mirDIP, microT-CDS, and miRDB). (**B**) GO analysis and enriched GO terms of 159 commonly differentially expressed targeted mRNAs on their biological process (BP), cellular component (CC), molecular function (MF). Top 20 GO enrichment terms were shown. (**C**) KEGG enrichment analysis of the association of miR-532-3p expression with enriched signalling pathways. Top 20 hits of the pathway enrichment analysis were shown. (**D** and **E**) Dual-luciferase assays demonstrated that the effect on TOP/FOP reporter activity in HEK-293T, MGC803, and AGS cells transfected with shRNA1 plasmid and sh-NC, circFGD4 overexpression plasmid and NC. (**F**) Dual-luciferase reporter assays indicated that the effect on TOP/FOP reporter activity in GC cells after transfection with miR-NC, miR-532-3p mimics or miR-532-3p inhibitors, circFGD4 overexpression plasmid or shRNA1 plasmid, and miR-532-3p mimics + circFGD4 overexpression plasmid or miR-532-3p inhibitors + shRNA1 plasmid. (**G**) Western blotting showed the total and nuclear β-catenin proteins in MGC803 and AGS cells after transfection with miR-NC, miR-532-3p mimics or miR-532-3p inhibitors, circFGD4 overexpression plasmid or shRNA1 plasmid, and miR-532-3p mimics + circFGD4 overexpression plasmid or miR-532-3p inhibitors + shRNA1 plasmid. GAPDH or Lamin B1 was used as an internal control and an endogenous control for the nuclear fraction, respectively. (**H**) Schematic diagram of the mechanism of the circFGD4/miR-532-3p axis in the regulation of GC proliferation, migration, and EMT by inhibiting the β-catenin signalling in an APC-modulated manner (values are shown as the mean ± standard error of the mean based on three independent experiments; $^{*}P<0.05$, $^{**}P<0.01$).

of both reduced this difference (Figure 6G). Also, similar nuclear/cytoplasmic ratios of β-catenin were examined in MGC803 cells transfected with miR-532-3p mimics and/or circFGD4 overexpressing vector (Figure 6G). These results indicated that circFGD4 decreased the aggregation of β-catenin in the nucleus of GC cells by suppressing miR-532-3p and facilitating APC expression, thereby inactivating the classical Wnt/β-catenin signalling pathway (Figure 6H).

Overexpression of circFGD4 suppressed GC tumorigenesis and metastasis *in vivo*

To explore the roles of circFGD4 on tumour growth, we established a mouse xenograft model. The nude mice were killed after 4 weeks; Xenograft tumours were excised and photographed (Figure 7A). In contrast with the negative control vector (NC) group, the xenograft tumours in the circFGD4 overexpression group indicated a decrease in volume and weight (Figure 7B,C). We conducted qRT-PCR assay on the collected tumours; the results showed that circFGD4 overexpression significantly reduced mRNA levels of miR-532-3p, Ki-67, PCNA, and Vimentin expression and increased APC and E-cadherin expression (Figure 7D). IHC assay was further performed; the results indicated that circFGD4 overexpression enhanced the immunochemical staining of APC and E-cadherin and reduced the immunostaining of Ki-67, PCNA, and Vimentin (Figure 7E). After that, to construct a lung metastasis model, the number and size of lung metastatic nodules were significantly lower in nude mouse injected by MGC803 cells with circFGD4 overexpressing group compared with that nude mouse injected with cells from blank or NC group (Figure 7F). Also, the mRNA levels of miR-532-3p, Ki-67, PCNA, and Vimentin in the circFGD4 overexpression group were lower than that in the NC group, while the APC, E-cadherin level was increased in circFGD4 overexpression group (Figure 7G). These data indicated that circFGD4 suppressed the tumorigenesis and metastasis of GC *in vivo*.

Discussion

A large number of circRNAs play essential roles as regulators and are valuable diagnostic markers for tumorigenesis and tumour progression [20]. For example, down-regulation of hsa_circ_0009361 has been detected in the cancerous tissues from colorectal cancer patients (CRC), and its use as a biomarker has been suggested, as low expression of hsa_circ_0009361 predicted cancer progression, metastasis and induced EMT of CRC patients [21]. Circular RNA cSMARCA5 is highly down-regulated in the tissues resected from hepatocellular cancer (HCC), and cSMARCA5 is correlated with advanced tumour stage and poor prognosis of HCC patients [22]. Here, we performed a circRNA microarray screen and selected circFGD4 to study its biological function further. We validated that circFGD4 was prominently reduced in GC tissues and cell lines and that lower expression of circFGD4 was markedly correlated with poor differentiation, lymphatic metastasis, and poor prognosis of GC patients. Functional experiments confirmed that circFGD4 inhibited tumour growth, metastasis, and induced EMT in GC cells. These data indicated that circFGD4 could act as a tumour suppressor in the tumorigenesis and metastasis of GC and might be a novel potential biomarker and therapeutic strategy for GC.

A growing number of studies have shown that cytoplasmic ncRNAs, including circRNAs, lncRNAs, and miRNAs, can affect mRNA stability and translation process or can regulate signalling pathways through competing with miRNAs for shared MREs [23–25]. In our study, preliminary bioinformatics analysis indicated that circFGD4 contained the MRE of miR-532-3p. Thus, we presumed that circFGD4 might play an anti-cancer effect through sponging miR-532-3p in GC. Subsequently, RNA FISH, dual-luciferase reporter gene, RNA immunoprecipitation, and circFGD4 pull-down assays demonstrated that circFGD4 interacted directly with miR-532-3p in GC. The rescue experiments further verified that circFGD4 inhibited tumour progression and metastasis by directly sponging miR-532 in GC. Next, we found that the APC gene, vital cell proliferation, and migration regulator, had a potential binding site for miR-532-3p according to bioinformatics analysis. We observed that circFGD4 not only regulated the expression level of APC in GC cells but that miR-532-3p also affected the expression of APC at the mRNA and protein levels, suggesting that the APC gene could probably be the target molecule of the circFGD4/miR-532-3p axis. Furthermore, dual-luciferase reporter assays determined that miR-532-3p could directly bind to APC. Western blotting and IF analysis indicated that circFGD4 could regulate the expression of APC via miR-532-3p, suggesting that circFGD4 inhibits GC progression through sponging miR-532-3p and thus regulating APC gene expression in GC cells.

Many works of literature have demonstrated that the Wnt/β-catenin signalling pathway is closely related to the viability, metastasis, and EMT of many malignant tumours [26,27]. The inhibition of the Wnt/β-catenin pathway by APC protein has been demonstrated in many studies [28,29]. Based on bioinformatics analysis, we found that cell migration and the Wnt signalling pathway were biological processes and pathways of miR-532-3p targeting genes. We further found that circFGD4 overexpression reduced the TOP/FOP activity, while knockdown of circFGD4 had the reverse effect; these results suggested that the Wnt/β-catenin signalling pathway was inactivated. Based on the further studies, increasing the miR-532-3p expression could significantly enhance the TOP/FOP transcriptional activity, suggesting that the Wnt/β-catenin signalling pathway was activated and cotransfection with circFGD4 shRNA1/circFGD4 overexpressed vector and miR-532-3p inhibitors/ mimics can enhance or reduce the TOP/FOP activity. Therefore, our data indicated that a novel circFGD4/miR-532-3p/APC regulatory network suppressed the progression and metastasis of GC by inactivating the β-catenin signalling.

Clinical Science (2020) **134** 1821–1839
https://doi.org/10.1042/CS20191043

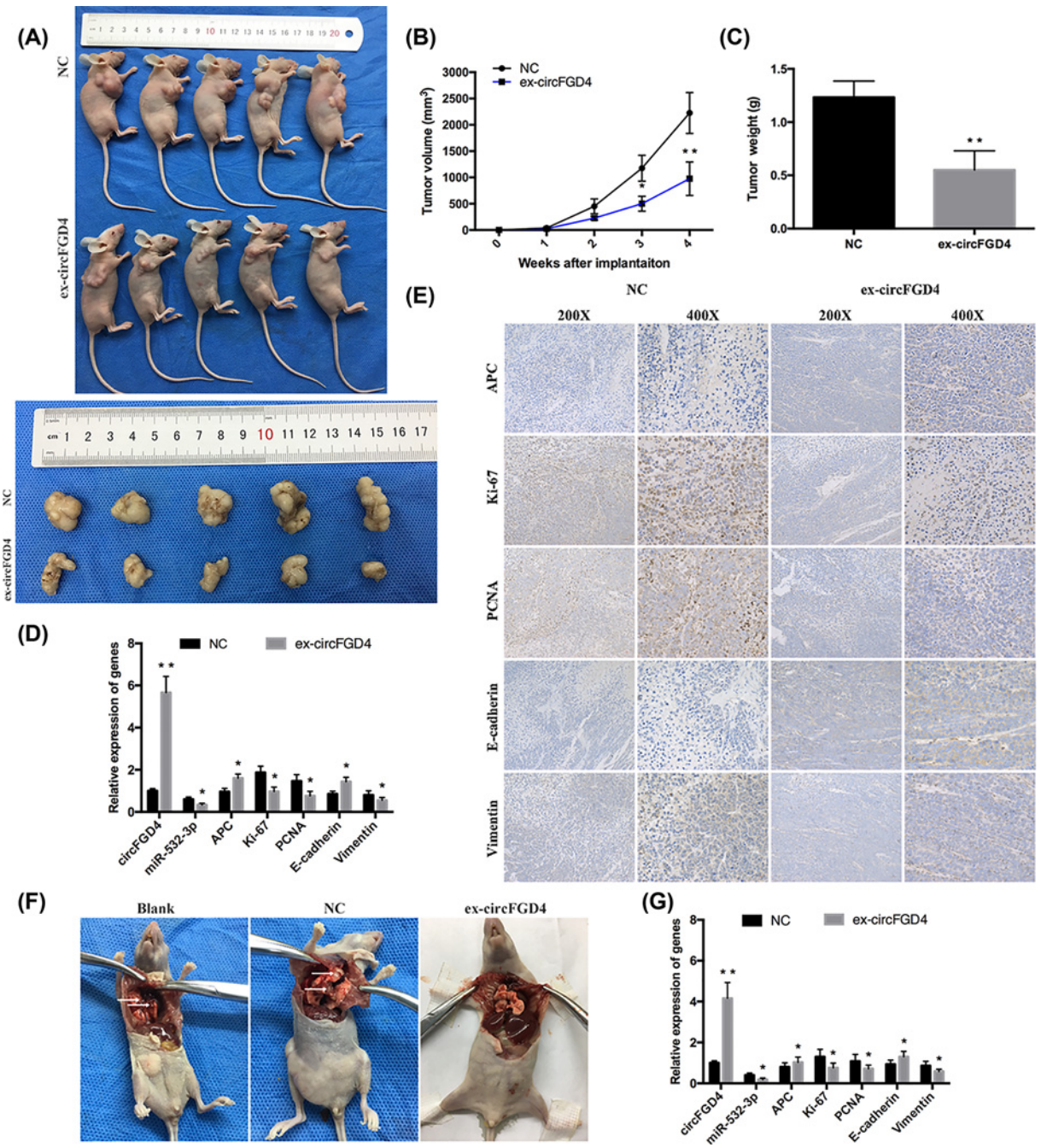

Figure 7. Overexpression of circFGD4 suppressed GC tumorigenesis and metastasis *in vivo*

(**A**) Representation images of tumour formation of xenograft in nude mice ($n = 5$/group) inoculated with MGC803 cells transfected with circFGD4 overexpression or a control vector (NC). (**B** and **C**) Tumour volume and weight of the xenograft tumours in the circFGD4 overexpression and NC groups. (**D**) qRT-PCR assays demonstrated the mRNA levels of circFGD4, miR-532-3p, APC, Ki-67, PCNA, E-cadherin, and Vimentin in tumours from the circFGD4 overexpression and control groups. (**E**) IHC assays revealed the structure of GC in mice and relative protein levels of APC, Ki-67, PCNA, E-cadherin, and Vimentin in tumours from the circFGD4 overexpression and control groups. (**F**) Representative images of lung metastatic nodules in the blank, NC, and circFGD4 overexpression groups are indicated by white arrows. (**G**) qRT-PCR assays determined the expression levels of circFGD4, miR-532-3p, APC, Ki-67, PCNA, E-cadherin, and Vimentin genes in lung metastasis from nude mouse in the NC and circFGD4 overexpression groups (values are shown as the mean ± standard error of the mean based on three independent experiments; $^{*}P<0.05$, $^{**}P<0.01$).

Conclusion

In summary, we demonstrated that circFGD4, which directly targets miR-532-3p/APC, suppressed GC cell viability, metastasis, and induced EMT through inactivating the β-catenin signalling. Our study suggests that circFGD4 serves a novel biomarker and therapeutic strategy for anti-GC therapy.

Clinical perspectives

- The roles of circRNAs in multiple cancers are not fully understood, and the underlying mechanisms by which circFGD4 contributed to gastric cancer (GC) remain mostly uncovered.
- We identified that circFGD4 was markedly down-regulated in GC, and lower expression of circFGD4 was correlated with the poor tumour differentiation, lymph node metastasis, and poor prognosis of GC patients. The low expression level of circFGD4 promoted the viability, migration, and induced EMT of GC cells. The mechanistic analysis demonstrated that circFGD4 suppressed GC progression through sponging miR-532-3p and enhancing APC expression to inactivate the β-catenin signalling.
- We identified a novel functional pathway controlled by the circFGD4/miR-532-3p/APC network. This regulatory network may provide a novel potential biomarker and valuable therapeutic strategy for GC.

Data Availability

All the data and materials supporting the conclusion of the present study have been included within the article.

Competing Interests

The authors declare that there are no competing interests associated with the manuscript.

Funding

This work was supported by the National Natural Science Foundation of China [grant number 81974385] and Chongqing Municipal Key Discipline Funding from the funding agencies of Chongqing Municipal Education Commission [grant number 201128GRJFJY].

Author Contribution

Xinglong Dai and Jianjun Liu substantially contributed to the conception and design of the work; Xiong Guo, Xiaoya Deng, and Anqi Cheng contributed to acquisition, analysis and interpretation of the data; Xinglong Dai drafted the manuscript; Xinglong Dai, Jianjun Liu, Xiong Guo, Anqi Cheng, Xiaoya Deng, Liqun Guo, and Ziwei Wang revising the work critically; all authors gave final approval of the work.

Ethics Approval

The Ethics Committee of the First Affiliated Hospital of Chongqing Medical University approved the study, and all participants signed informed consent statements. All animal experiments were approved by the Animal Ethics Committee of Chongqing Medical University.

Abbreviations

APC, adenomatous polyposis coli; CCK-8, Cell Counting Kit-8; circFGD4, circular RNA FGD4; circRNA, circular RNA; DAB, diaminoaniline; DAPI, 4′,6-Diamidino-2-phenylindole; EdU, 5-Ethynyl-2′-deoxyuridine; EMT, epithelial–mesenchymal transition; FISH, fluorescence *in situ* hybridization; GAPDH, glyceraldehyde 3-phosphate dehydrogenase; GC, gastric cancer; HRP, horseradish peroxidase; IF, immunofluorescence; IHC, immunohistochemistry; MREs, miRNA response elements; MUT, mutant-type; PVDF, polyvinylidene fluoride; qRT-PCR, quantitative real-time PCR; RIP, RNA immunoprecipitation; UTR, untranslated region; WT, wild-type.

Clinical Science (2020) **134** 1821–1839
https://doi.org/10.1042/CS20191043

References

1 Bray, F., Ferlay, J., Soerjomataram, I., Siegel, R.L., Torre, L.A. and Jemal, A. (2018) Global cancer statistics 2018: GLOBOCAN estimates of incidence and mortality worldwide for 36 cancers in 185 countries. *CA Cancer J. Clin.* **68**, 394–424, https://doi.org/10.3322/caac.21492

2 Chen, W., Zheng, R., Baade, P.D., Zhang, S., Zeng, H., Bray, F. et al. (2016) Cancer statistics in China, 2015. *CA Cancer J. Clin.* **66**, 115–132, https://doi.org/10.3322/caac.21338

3 Mihmanli, M., Ilhan, E., Idiz, U.O., Alemdar, A. and Demir, U. (2016) Recent developments and innovations in gastric cancer. *World J. Gastroenterol.* **22**, 4307–4320, https://doi.org/10.3748/wjg.v22.i17.4307

4 Allemani, C., Weir, H.K., Carreira, H., Harewood, R., Spika, D., Wang, X.S. et al. (2015) Global surveillance of cancer survival 1995-2009: analysis of individual data for 25,676,887 patients from 279 population-based registries in 67 countries (CONCORD-2). *Lancet* **385**, 977–1010, https://doi.org/10.1016/S0140-6736(14)62038-9

5 Qi, X., Zhang, D.H., Wu, N., Xiao, J.H., Wang, X. and Ma, W. (2015) ceRNA in cancer: possible functions and clinical implications. *J. Med. Genet.* **52**, 710–718, https://doi.org/10.1136/jmedgenet-2015-103334

6 Kristensen, L.S., Hansen, T.B., Venø, M.T. and Kjems, J. (2018) Circular RNAs in cancer: opportunities and challenges in the field. *Oncogene* **37**, 555–565, https://doi.org/10.1038/onc.2017.361

7 Memczak, S., Jens, M., Elefsinioti, A., Torti, F., Krueger, J., Rybak, A. et al. (2013) Circular RNAs are a large class of animal RNAs with regulatory potency. *Nature* **495**, 333–338, https://doi.org/10.1038/nature11928

8 Li, Y., Zheng, Q., Bao, C., Li, S., Guo, W., Zhao, J. et al. (2015) Circular RNA is enriched and stable in exosomes: a promising biomarker for cancer diagnosis. *Cell Res.* **25**, 981–984, https://doi.org/10.1038/cr.2015.82

9 Abdelmohsen, K., Panda, A.C., Munk, R., Grammatikakis, I., Dudekula, D.B., De, S. et al. (2017) Identification of HuR target circular RNAs uncovers suppression of PABPN1 translation by CircPABPN1. *RNA Biol.* **14**, 361–369, https://doi.org/10.1080/15476286.2017.1279788

10 Li, Z., Yanfang, W., Li, J., Jiang, P., Peng, T., Chen, K. et al. (2018) Tumour-released exosomal circular RNA PDE8A promotes invasive growth via the miR-338/MACC1/MET pathway in pancreatic cancer. *Cancer Lett.* **432**, 237–250, https://doi.org/10.1016/j.canlet.2018.04.035

11 Tian, L., Cao, J., Jiao, H., Zhang, J., Ren, X., Liu, X. et al. (2019) CircRASSF2 promotes laryngeal squamous cell carcinoma progression by regulating the miR-302b-3p/IGF-1R axis. *Clin. Sci. (Lond.)* **133**, 1053–1066, https://doi.org/10.1042/CS20190110

12 Dang, Y., Ouyang, X., Zhang, F., Wang, K., Lin, Y., Sun, B. et al. (2017) Circular RNAs expression profiles in human gastric cancer. *Sci. Rep.* **7**, 9060, https://doi.org/10.1038/s41598-017-09076-6

13 Zhang, Z., Liu, S., Shi, R. and Zhao, G. (2011) miR-27 promotes human gastric cancer cell metastasis by inducing epithelial-to-mesenchymal transition. *Cancer Genet.* **204**, 486–491, https://doi.org/10.1016/j.cancergen.2011.07.004

14 Glažar, P., Papavasileiou, P. and Rajewsky, N. (2014) circBase: a database for circular RNAs. *RNA* **20**, 1666–1670, https://doi.org/10.1261/rna.043687.113

15 Dudekula, D.B., Panda, A.C., Grammatikakis, I., De, S., Abdelmohsen, K. and Gorospe, M. (2016) CircInteractome: A web tool for exploring circular RNAs and their interacting proteins and microRNAs. *RNA Biol.* **13**, 34–42, https://doi.org/10.1080/15476286.2015.1128065

16 Liu, M., Wang, Q., Shen, J., Yang, B.B. and Ding, X. (2019) Circbank: a comprehensive database for circRNA with standard nomenclature. *RNA Biol.* **16**, 899–905, https://doi.org/10.1080/15476286.2019.1600395

17 Chang, T.H., Huang, H.Y., Hsu, J.B., Weng, S.L., Horng, J.T. and Huang, H.D. (2013) An enhanced computational platform for investigating the roles of regulatory RNA and for identifying functional RNA motifs. *BMC Bioinformatics* **14**, S4, https://doi.org/10.1186/1471-2105-14-S2-S4

18 Xia, S., Feng, J., Chen, K., Ma, Y., Gong, J., Cai, F. et al. (2018) CSCD: a database for cancer-specific circular RNAs. *Nucleic Acids Res.* **46**, D925–D929, https://doi.org/10.1093/nar/gkx863

19 Huang, D.W., Sherman, B.T. and Lempicki, R.A. (2009) Systematic and integrative analysis of large gene lists using DAVID Bioinformatics Resources. *Nat. Protoc.* **4**, 44–57, https://doi.org/10.1038/nprot.2008.211

20 Kulcheski, F.R., Christoff, A.P. and Margis, R. (2016) Circular RNAs are miRNA sponges and can be used as a new class of biomarker. *J. Biotechnol.* **238**, 42–51, https://doi.org/10.1016/j.jbiotec.2016.09.011

21 Geng, Y., Zheng, X., Hu, W., Wang, Q., Xu, Y., He, W. et al. (2019) Hsa_circ_0009361 acts as the sponge of miR-582 to suppress colorectal cancer progression by regulating APC2 expression. *Clin. Sci. (Lond.)* **133**, 1197–1213, https://doi.org/10.1042/CS20190286

22 Yu, J., Xu, Q.G., Wang, Z.G., Yang, Y., Zhang, L., Ma, J.Z. et al. (2018) Circular RNA cSMARCA5 inhibits growth and metastasis in hepatocellular carcinoma. *J. Hepatol.* **68**, 1214–1227, https://doi.org/10.1016/j.jhep.2018.01.012

23 Verduci, L., Strano, S., Yarden, Y. and Blandino, G. (2019) The circRNA-microRNA code: emerging implications for cancer diagnosis and treatment. *Mol. Oncol.* **13**, 669–680, https://doi.org/10.1002/1878-0261.12468

24 Wang, Z., Ma, K., Pitts, S., Cheng, Y., Liu, X., Ke, X. et al. (2018) Novel circular RNA NF1 acts as a molecular sponge, promoting gastric cancer by absorbing miR-16. *Endocr. Relat. Cancer* **26**, pii: ERC–18-0478.R1

25 Yang, X.Z., Cheng, T.T., He, Q.J., Lei, Z.Y., Chi, J., Tang, Z. et al. (2018) LINC01133 as ceRNA inhibits gastric cancer progression by sponging miR-106a-3p to regulate APC expression and the Wnt/β-catenin pathway. *Mol. Cancer* **17**, 126, https://doi.org/10.1186/s12943-018-0874-1

26 Huang, J., Xiao, D., Li, G., Ma, J., Chen, P., Yuan, W. et al. (2014) EphA2 promotes epithelial-mesenchymal transition through the Wnt/β-catenin pathway in gastric cancer cells. *Oncogene* **33**, 2737–2747, https://doi.org/10.1038/onc.2013.238

27 Wu, C., Zhuang, Y., Jiang, S., Liu, S., Zhou, J., Wu, J. et al. (2016) Interaction between Wnt/β-catenin pathway and microRNAs regulates epithelial-mesenchymal transition in gastric cancer (Review). *Int. J. Oncol.* **48**, 2236–2246, https://doi.org/10.3892/ijo.2016.3480

28 Xu, M., Liu, X., Xu, Y., Zhu, S. and Gao, Y. (2017) Co-expression of Axin and APC gene fragments inhibits colorectal cancer cell growth via regulation of the Wnt signaling pathway. *Mol. Med. Rep.* **16**, 3783–3790, https://doi.org/10.3892/mmr.2017.7049

29 Lee, E., Salic, A., Krüger, R., Heinrich, R. and Kirschner, M.W. (2003) The roles of APC and Axin derived from experimental and theoretical analysis of the Wnt pathway. *PLoS Biol.* **1**, E10, https://doi.org/10.1371/journal.pbio.0000010